Mineralogical Magazine, April 2018, Vol. 82(2), pp. 275–290

Embreyite: structure determination, chemical formula and comparative crystal chemistry

VADIM M. KOVRUGIN[1,2], OLEG I. SIIDRA[1,3,*], IGOR V. PEKOV[4], NIKITA V. CHUKANOV[5], DMITRY A. KHANIN[4] AND ATALI A. AGAKHANOV[6]

[1] Department of Crystallography, St Petersburg State University, University emb. 7/9, 199034 St Petersburg, Russia
[2] Laboratoire de Réactivité et Chimie des Solides, UMR 7314 CNRS, Université de Picardie Jules Verne, 33 rue St Leu, 80039 Amiens, France
[3] Nanomaterials Research Center, Kola Science Center, Russian Academy of Sciences, Apatity, 184200, Murmansk Region, Russia
[4] Faculty of Geology, Moscow State University, Vorobievy Gory, 119991 Moscow, Russia
[5] Institute of Problems of Chemical Physics, Russian Academy of Sciences, Chernogolovka, Moscow Region, 142432, Russia
[6] Fersman Mineralogical Museum of the Russian Academy of Sciences, Leninsky Prospekt 18-2, 119071 Moscow, Russia

[*Received 29 November 2016; Accepted 24 May 2017; Associate Editor: Juraj Majzlan*]

ABSTRACT

Embreyite from the Berezovskoe, Urals, Russia, was studied by the means of powder X-ray diffraction (XRD), single-crystal XRD, infrared spectroscopy and microprobe analysis. The empirical formula of embreyite obtained on the basis of microprobe analysis is $Pb_{1.29}Cu_{0.07}Cr_{0.52}P_{0.43}O_4$ (without taking into account the presence of H_2O). An examination of single-crystal XRD frames of the tested crystals cut from embreyite intergrowths revealed split reflection spots of weak intensities, even after a long exposure time. The crystal structure of embreyite (monoclinic, *C*2/*m*, $a = 9.802(16)$, $b = 5.603(9)$, $c = 7.649(12)$ Å, $\beta = 114.85(3)^o$ and $V = 381.2(11)$ Å^3) has been solved by direct methods and refined to $R_1 = 0.050$ for 318 unique observed reflections. The powder XRD patterns of the holotype embreyite and the fresh material studied are close in both *d* values and the intensities match the pattern calculated from the structural single-crystal XRD data. The unit-cell parameters were re-calculated for the holotype sample using a new cell setting and corresponding *hkl* indices. The crystal structure of embreyite is based on layers formed by corner-sharing mixed chromate-phosphate tetrahedra and PbO_6 distorted octahedra. The interlayer space is filled by disordered Pb^{2+} and Cu^{2+} cations. Generally, the crystal structure of embreyite can be referred to the structural type of palmierite. $\{Pb[(Cr,P)O_4]_2]\}$ layers in embreyite are similar in topology to those in yavapaiite-type compounds. The general formula of embreyite can be represented as $(Pb_xM^{2+}_y\square_{1-x-y})_2\{Pb[(Cr,P)O_4]_2\}(H_2O)_n$, where M^{2+} = Cu and Zn and $0.5 \leq x+y \leq 1$, or, in the simplified form: $(Pb,Cu,\square)_2\{Pb[(Cr,P)O_4]_2\}(H_2O)_n$. The simplified formula of embreyite is similar in stoichiometry to vauquelinite and may explain the existence of the solid-solution series. The determination of the crystal structure of embreyite may also help to resolve the crystal chemical nature of cassedanneite. The XRD pattern of cassedanneite contains a distinct reflection with $d = 13.9$ Å, forbidden for the embreyite unit cell. This feature may indicate the doubling of the *c* unit-cell parameter of cassedanneite in comparison with embreyite. We assume that cassedanneite has structural similarity to embreyite with, presumably, a disordered distribution of Cr and V.

KEYWORDS: embreyite, layered structure, lead, chromate, phosphate, vauquelinite, cassedanneite, oxidation zone, Berezovskoe deposit, Urals.

*E-mail: o.siidra@spbu.ru
https://doi.org/10.1180/minmag.2017.081.041

Introduction

EMBREYITE was described as a new mineral species in old museum collection samples from the Berezovskoe deposit, Central Urals, Russia by Williams (1972). [Note: Williams reports the locality as "Berezov, Siberia". According to old museum labels, geographical maps and 18–19th century literature, the Urals was typically included in Siberia]. This deposit, discovered in 1745, is located near the city of Ekaterinburg and is currently still being mined for gold. Berezovskoe is world-famous for historical mineralogical objects because of outstanding, very rich and diverse chromate mineralization in the oxidation zone. Berezovskoe is the type locality of five Pb chromate minerals: crocoite (discovered in 1766), vauquelinite (1818), phoenicochroite (1833), embreyite (1972) and cassedanneite (1988). Crocoite was the first new mineral species described from Russia and chromium was discovered in samples of this mineral from Berezovskoe in 1797 by L.N. Vauquelin (see Pekov, 1998 and references therein).

The chemical composition, powder XRD and physical properties were well determined for the type material of embreyite. However, all of the crystals were too low quality for single-crystal X-ray studies. Crystals of the original embreyite were described as thin plates consisting of sub-individuals oriented differently relative to each other and, additionally, split. The idealized formula of the mineral based on chemical data obtained by different methods was reported as $Pb_5(CrO_4)_2(PO_4)_2{\cdot}H_2O$. All of the analyses of the type material detected Pb^{2+}, Cr^{6+}, P, O and H as the main constituents. Cu^{2+} was also identified in the range of 1.2–2.5 (average 1.7) wt.% CuO (Williams, 1972). Additional recent studies of embreyite from the Berezovskoe ore field (several mines) and two other Ural localities (Mt. Bertevaya near the city of Nizhniy Tagil and Mt. Sukhovyaz within the city of Verkhniy Ufaley) revealed significant chemical variations (in wt.%): PbO 68.1–77.9, CuO 0.6–6.9, ZnO 0.0–1.9, P_2O_5 6.4–9.7, As_2O_5 0.0–2.6 and CrO_3 9.1–15.0 (Kleymenov *et al.*, 2003; Khanin *et al.*, 2015). It was found that embreyite forms a continuous solid-solution series with vauquelinite, despite the difference in powder XRD patterns. Many of the recently obtained electron-microprobe analyses (EMPA) of embreyite are not in good agreement with the original idealized formula of $Pb_5(CrO_4)_2(PO_4)_2{\cdot}H_2O$. The following generalized formula was suggested, taking into account all of the additional studies: $Pb_2[Pb_x,M^{2+}_y,\square_{1-x-y}]_{\Sigma1}(CrO_4)(PO_4)(OH_{2(x+y)-1},H_2O,\square)_{\Sigma1}$, where M^{2+} = Cu or Zn, $\square$ = vacancy and $0.5 \leq x+y \leq 1$; simplified as $Pb_2(M,\square)(CrO_4)(PO_4)X$, where M = Pb, Cu or Zn and X = OH, H_2O or $\square$ (Khanin *et al.*, 2015). However, the latter formula could not be proven due to the lack of a single-crystal XRD study.

Embreyite is a member of a rather small group of lead-containing minerals with $(CrO_4)^{2-}$ anions (Table 1). Note that Pb chromates are the richest group for chromate minerals in general. Chromium mineral diversity is on the lower limit of the common trend as a function of the crustal abundance of Cr (Christy, 2015). A relatively small number of described chromate mineral species to date can be explained generally by the instability of the $(CrO_4)^{2-}$ anion and the tendency of Cr^{6+} to reduce under conventional natural conditions. There have been several attempts to study the crystal structure of embreyite during the more than 40 years since its discovery. They were all unsuccessful due to the low quality of crystals. Crystals suitable for a structure determination were found in samples (Fig. 1) collected in 2011 at Berezovskoe by I.V.P. Herein, we report the determination of the structural features of embreyite and discuss relationships with the other Pb chromate minerals and synthetic phases.

Experimental

Sample description

The sample used in this study was found in the 'Krokoitovyi Shurf' (Crocoite Pit) at Mt. Uspenskaya in the area of the former Tsvetnoy Mine, the type locality of crocoite. This mine was operated from 1752 to 1802, and is situated in the central part of the Berezovskoe ore field. The richest secondary mineralization is located at a depth of ~12 m below surface. It is distributed in an area consisting mainly of partially weathered beresites and listwanites (Fettes and Desmons, 2007) with numerous quartz veins containing abundant cavities. Some of the latter are formed after dissolved pyrite, galena and 'fahlerz', as well as cavernous open-work polycomponent pseudomorphs consisting of the supergene minerals. The assemblage of secondary minerals associated intimately with embreyite examined in the course of this study includes crocoite, vauquelinite (two morphological and colour varieties: greenish-black spherical crystal clusters and olive-green fine-grained crusts and kidney-shaped aggregates), pyromorphite, goethite (limonite) and

https://doi.org/10.1180/minmag.2017.081.041 Published online by Cambridge University Press

TABLE 1. List of Pb chromate minerals.

Mineral	Formula	Ref.
Cassedanneite	$Pb_5(VO_4)_2(CrO_4)_2 \cdot H_2O$ unknown crystal structure	[1]
Chromschieffelinite	$Pb_{10}Te_6O_{20}(OH)_{14}(CrO_4) \cdot 5H_2O$	[2]
Crocoite	$PbCrO_4$	[3, 4]
Embreyite	$Pb_2(Pb,Cu,\square)[(Cr,P)O_4]_2(H_2O,OH,\square)$	[5, 6, *]
Fornacite	$Pb_2Cu(CrO_4)(AsO_4)(OH)$	[6–9]
Georgerobinsonite	$Pb_4(CrO_4)_2(OH)_2FCl$	[10]
Hemihedrite	$Pb_{10}Zn(CrO_4)_6(SiO_4)_2F_2$	[8, 11, 12]
Iranite	$Pb_{10}Cu(CrO_4)_6(SiO_4)_2(OH)_2$	[8, 13–15]
Macquartite	$Pb_7Cu_2(CrO_4)_4(SiO_4)_2(OH)_2$ no single crystal X-ray data	[16, 17]
Phoenicochroite	$Pb_2O(CrO_4)$	[8, 18]
Reynoldsite	$Pb_2Mn_2O_5(CrO_4)$	[19]
Santanaite	$Pb_9^{2+}Pb_2^{4+}O_{12}(CrO_4)$ unknown crystal structure	[20]
Vauquelinite	$Pb_2Cu(CrO_4)(PO_4)(OH)$	[6, 8, 21]

References: [1] – Cesbron *et al*. (1988); [2] – Kampf *et al*. (2012*a*); [3] – Quareni and de Pieri (1965); [4] – Effenberger and Pertlik (1986); [5] – Williams (1972); [6] – Khanin *et al*. (2015); [7] – Cocco *et al*. (1967); [8] – Cesbron and Williams (1980); [9] – Ksenofontov *et al*. (2014); [10] – Cooper *et al*. (2011); [11] – Williams and Anthony (1970); [12] – McLean and Anthony (1970); [13] – Bariand and Herpin (1963); [14] – Adib and Ottemann (1970); [15] – Yang *et al*. (2007); [16] –Williams and Duggan (1980); [17] – Cooper and Hawthorne (1994); [18] – Williams *et al*. (1970); [19] – Kampf *et al*. (2012*b*); [20] – Mücke (1972); [21] – Fanfani and Zanazzi (1968); * – this work.

undetermined clay mineral(s). Embreyite occurs as flattened, coarse hexagonal, typically roundish, disc-like crystals up to 0.3 mm and, rarely, up to 1 mm across (Fig. 1). They are usually divergent, resembling an open book, and combined in groups or crusts up to 3 mm × 3 mm and up to 1 mm thick. The mineral is orange to yellow orange, sometimes brownish-yellow, with a strong greasy lustre. Embreyite is one of the latest minerals of this assemblage overgrowing crocoite and pyromorphite.

FIG. 1. Aggregates of brown-orange embreyite crystals (in the centre) with crocoite (bright orange prismatic crystals) and pyromorphite (yellow-green) around. Field of view: width = 5.8 mm. Photo: A.V. Kasatkin.

Chemical composition

The chemical composition was determined for the embreyite crystal used for the structure determination on a Jeol 733 electron microprobe instrument operating in energy-dispersive mode with an accelerating voltage of 20 kV, a beam current of 2 nA and a beam diameter of 5 μm. The X-ray acquisition live-time was 30 s. The following standards were used: $PbTiO_3$ (Pb), Cu metal (Cu), chromite USNM 117075 (Cr) and $LaPO_4$ (P). The average (four spot analyses) chemical composition (wt.%, ranges in parentheses) is: PbO 74.46 (73.79–75.04), CuO 1.38 (1.18–1.51), CrO_3 13.40 (13.06–13.71) and P_2O_5 7.96 (7.78–8.10),

https://doi.org/10.1180/minmag.2017.081.041 Published online by Cambridge University Press

total 97.20. Contents of other elements with atomic numbers higher than carbon are below detection limits. The H_2O content was not determined because of paucity of the material. The empirical formula calculated on the basis of 4 O atoms per formula unit (apfu) (without taking into account the possible presence of some H_2O: see below) is: $Pb_{1.29}Cu_{0.07}Cr_{0.52}P_{0.43}O_4$.

Infrared spectroscopy

In order to obtain the infrared (IR) absorption spectrum (Fig. 2), a powdered sample of embreyite was mixed with dried KBr, pelletized and analysed using a Bruker ALPHA FTIR spectrometer with a resolution of 4 cm^{-1} and 16 scans. The IR spectrum of a pellet of pure KBr was used as a reference.

Note, most of the Pb–O vibrations are expected to be in the region below 300 cm^{-1} and were not registered in the region of the IR spectra studied. Absorption bands in the IR spectrum of embreyite and their assignments are (cm^{-1}; s – strong band, sh – shoulder): 3329 and diffuse absorption between 3100 and 3300 [O–H stretching vibrations of H_2O molecules], 1680w [bending vibrations of H_2O molecules], 1418, 1356 [probably vibrations of H^+ cations], 1030sh, 959s [$\nu_3(F_2)$ – asymmetric P–O stretching vibrations of PO_4^{3-} anions], 900sh [$\nu_1(A_1)$ – symmetric P–O stretching vibrations of PO_4^{3-} anions], 855s, 830sh [$\nu_3(F_2)$ – asymmetric Cr–O stretching vibrations of CrO_4^{2-} anions], 560sh, 538 [triply degenerate $\nu_4(F_2)$ O–P–O bending mode of PO_4^{3-} anions], 418w, 383 [lattice modes involving $\nu_2(E)$ O–P–O bending vibrations, possibly combined with vibration modes of H_2O molecules]. The band assignments were done according to Nakamoto (2009) and Chukanov and Chervonnyi (2016).

Powder XRD

Powder XRD data of embreyite were collected with a Rigaku R-AXIS Rapid II single-crystal diffractometer equipped with cylindrical image plate detector using Debye-Scherrer geometry (d = 127.4 mm, Co$K\alpha$ radiation and λ = 1.7890 Å). The powder XRD pattern and unit-cell parameters refined from the powder data are given in Table 2 and compared with the data for the holotype sample reported by Williams (1972).

Single-crystal XRD

Single crystals of embreyite were examined under an optical microscope, mounted on glass fibers with epoxy and tested on a Bruker APEX DUO diffractometer equipped with a micro-focus X-ray tube operated with Mo$K\alpha$ radiation (λ = 0.71073 Å) at 50 kV and 40 mA. An examination of XRD frames of the tested crystals cut from embreyite intergrowths revealed split reflection spots of weak intensities, even after a long exposure time. The quality of the crystals of embreyite made the solution of the crystal structure challenging. An orange translucent platy crystal, 0.14 mm ×

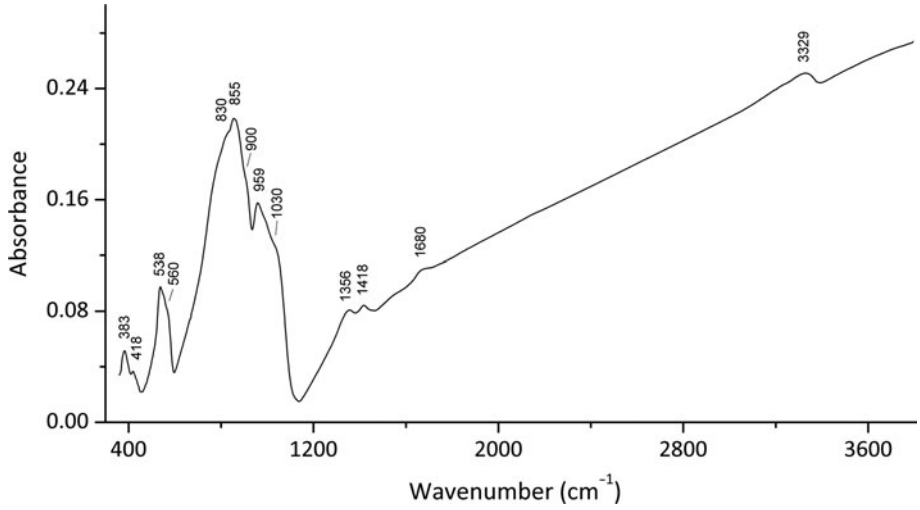

FIG. 2. Infrared (FTIR) spectrum for the embreyite sample studied in this work.

https://doi.org/10.1180/minmag.2017.081.041 Published online by Cambridge University Press

TABLE 2. Powder XRD data and unit-cell parameters of embreyite.

This work		Holotype specimen*		This work**		*h k l*
I_{obs}	d_{obs}, Å	I_{obs}	d_{obs}, Å	d_{calc}, Å	I_{calc}	
6	6.92	3	6.941	6.941	2	001
48	4.738	60	4.751	4.763, 4.741	25, 40	$\bar{2}01$, 110
8	4.377	3	4.378	4.401	1	$\bar{1}11$
15	3.550	32	3.563	3.561, 3.555	11, 4	111, $\bar{2}02$
15	3.471	28	3.475	3.470	10	002
100	3.157	100	3.167	3.185, 3.158	54, 100	201, $\bar{1}12$
44	2.813	60	2.818	2.822, 2.801	55, 24	$\bar{3}11$, 020
8	2.599	17	2.608	2.620, 2.609, 2.598	4, 3, 4	310, $\bar{3}12$, 021
4	2.547			2.542	1	112
1	2.409	4	2.407	2.415	1	$\bar{2}21$
4	2.320	23	2.314	2.314	3	003
8	2.254	32	2.213	2.224	8	400
14	2.194	31	2.187	2.200, 2.197, 2.183, 2.180	12, 3, 5, 3	$\bar{2}22$, 311, $\bar{3}13$, 022
19	2.099	31	2.105	2.105, 2.104	7, 12	$\bar{4}03$, 221
24	1.910	45	1.917	1.917, 1.911	14, 7	113, $\bar{2}04$
9	1.848			1.842	2	$\bar{5}12$
4	1.833			1.838, 1.828	1, 1	$\bar{4}21$, 130
3	1.795			1.795	2	312
7	1.780	26	1.789	1.784, 1.784, 1.780, 1.777	1, 1, 2, 1	023, $\bar{3}14$, 222, $\bar{4}04$
2	1.760			1.762	1	$\bar{1}14$
2	1.735			1.735	1	004
6	1.692			1.695	4	510
5	1.681			1.683, 1.678	3, 2	$\bar{4}23$, $\bar{1}32$
2	1.641			1.634	1	$\bar{6}02$
3	1.617			1.621	2	$\bar{3}31$
7	1.577			1.580, 1.579, 1.578	1, 3, 2	330, $\bar{2}24$, $\bar{3}32$
1	1.497			1.501, 1.499	1, 1	$\bar{4}24$, $\bar{1}33$
3	1.410			1.411	2	$\bar{6}22$
4	1.403			1.401	1	040
4	1.386			1.385	1	422
5	1.378			1.378, 1.377, 1.373	1, 1, 1	$\bar{5}15$, 133, 041
4	1.335			1.342, 1.339, 1.336	1, 1, 1	$\bar{5}31$, 601, 240
2	1.325			1.325	2	$\bar{3}34$
4	1.306			1.307, 1.303	1, 1	$\bar{5}33$, $\bar{2}42$
Unit-cell parameters						
Calculated from powder XRD data		Calculated from powder XRD data		Determined by single crystal XRD data		
9.814(6)		9.75(1)		9.802(16)		*a*, Å
5.597(1)		5.604(4)		5.603(9)		*b*, Å
7.643(5)		7.635(9)		7.649(12)		*c*, Å
114.79(4)		114.48(9)		114.85(3)		β, °
381.1(4)		379.8(9)		381.2(11)		*V*, Å^3

*Holotype specimen: I_{obs} and d_{obs} values are after Williams (1972) and unit-cell parameters provided in this table were refined using the *hkl* indices of our calculated XRD pattern (the unit-cell data reported by Williams (1972) are: a = 9.755(3), b = 5.636(3), c = 7.135(3) Å, β = 103.8(3)° and V = 382 Å^3)
**XRD pattern calculated from our crystal-structure data.

https://doi.org/10.1180/minmag.2017.081.041 Published online by Cambridge University Press

0.12 mm × 0.07 mm demonstrating the best diffraction pattern (Fig. 3) was chosen for full XRD collection. More than a hemisphere of XRD data were collected with a frame width of 0.5° in ω and 60 s counting time for each frame. The data were integrated and corrected for absorption using a multi-scan-type model using the Bruker programs *APEX* and *SADABS*.

The unit-cell parameters of embreyite were determined and refined by the least-squares technique on the basis of 1334 reflections with 2θ in the range of 8.6–57.4°. The obtained unit-cell parameters (Table 2, 3) are in a good agreement with those previously reported in the $P2_1/m$ space group by Williams (1972). The $|E^2-1|$ parameter was equal to 0.899, which indicated high probability of a centrosymmetric space group confirmed by subsequent structure solution and refinement. The crystal structure of embreyite was solved in $C2/m$ using direct methods and refined to $R_1 = 0.050$ by means of the *SHELX* program package (Sheldrick, 2015). Crystallographic information is summarized in Table 3. Attempts to solve and refine the crystal structure in the higher symmetry space group, $R\bar{3}m$ ($a = 5.618(9)$, $c = 20.80(4)$ Å and $V = 569(2)$ Å^3), reported for the structure of rhombohedral polymorph of $Pb_4(PO_4)_2(CrO_4)$ (Barbier and Maxin, 1995) led us to a worse agreement between the crystallographic model and the experimental XRD data ($R_1 = 0.072$) and in addition significant disorder in the heteropolyhedral layer (see below) not observed in $C2/m$. Various twin laws in both space groups were tried but none of them appeared

TABLE 3. Crystallographic data for embreyite.

Crystal data	
Crystal system	monoclinic
Space group	$C2/m$
Unit-cell dimensions	
a (Å)	9.802(16)
b (Å)	5.603(9)
c (Å)	7.649(12)
α, β, γ (°)	90, 114.85(3), 90
Unit-cell volume (Å^3)	381.2(11)
Z	1
Calc. density (g·cm^{-3})	6.564
Absorption coef. (mm^{-1})	58.99
Crystal size (mm)	0.14 × 0.12 × 0.07
Data collection	
Temperature (K)	293
Radiation, wavelength (Å)	Mo$K\alpha$, 0.71073
F(000)	636
θ range (°)	4.3–28.7
h, k, l ranges	$-11 \le h \le 12$ $-7 \le k \le 5$ $-10 \le l \le 5$
Total refl. collected	1334
Unique refl. (R_{int})	500 (0.0471)
Unique refl. $F > 4\sigma(F)$	318
Structure refinement	
Refinement method	Full-matrix least-squares on F^2
Weighting coef. a, b	0.0794, 0
Data/restraints/parameters	500/0/55
R_1 [$F > 4\sigma(F)$],	0.0505
wR_2 [$F > 4\sigma(F)$]	0.1278
R_1 all, wR_2 all	0.0845, 0.1435
Goof on F^2	1.006
Largest diff. peak and hole (e Å^{-3})	1.358, −0.943

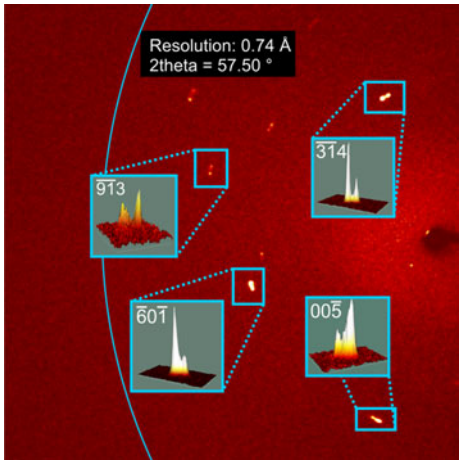

FIG. 3. Typical XRD frame of embreyite collected with width = 0.5° and 60 s of exposure.

to be successful and improved the refinement. Therefore, we provide here a description of the structure of embreyite in the monoclinic space group $C2/m$ as it resulted in a lower R-factor, very good fit with powder XRD patterns, better displacement parameters of atoms, and physically realistic interatomic bond-distance values.

A procedure of the structure refinement of embreyite included the following steps: (1) an initial group of the atom sites was determined by direct methods; (2) missing atoms were found from the difference-Fourier maps; (3) the structural model was refined until the atomic arrangements became reasonable; and (4) site occupancies were adjusted in accordance with the chemical data. All positions except the low occupied Cu one (site-occupation factor = 0.132) were refined

https://doi.org/10.1180/minmag.2017.081.041 Published online by Cambridge University Press

TABLE 4. Fractional atomic coordinates, site occupancy factors (SOF), bond-valence sums (vu) and equivalent or isotropic displacement parameters (Å^2) of atoms in the structure of embreyite.

Site	Atom	Wyck.	SOF	*x*	*y*	*z*	U_{iso}*/U_{eq}
Pb1*	Pb	2*d*	1	½	0	½	0.0891(7)
Pb2A**	Pb	4*i*	0.308	0.7919(5)	½	0.8693(4)	0.0729(8)
Pb2B	Pb	8*j*	0.189	0.7681(3)	0.6375(4)	0.9348(4)	0.0449(7)
Pb2C	Pb	4*i*	0.108	0.9074(7)	½	0.9379(8)	0.0372(12)
Cu1	Cu	2*b*	0.132	0	½	0	0.061(7)*
*T***	Cr	4*i*	0.520	0.9014(3)	0	0.7033(4)	0.0355(8)
	P		0.432				
O1	O	8*j*	1	0.0009(10)	0.2324(14)	0.7839(12)	0.055(2)
O2	O	4*i*	1	0.7725(14)	0	0.7787(19)	0.057(3)
O3	O	4*i*	1	0.8271(15)	0	0.4762(16)	0.071(4)

*Bond valence sum is 2.14 vu.
**Overall weighted bond-valence sums for disordered sites: Pb2 = 1.84 vu, *T* = 5.52 vu.
Wyck – Wyckoff positions.

anisotropically. Final atom coordinates and site-occupation factors are represented in Table 4. Selected bond distance values are in Table 5.

Results

Cation coordination

There are one fully occupied Pb1 site, one tetrahedrally coordinated *T* site and four oxygen sites in the heteropolyhedral layer in the crystal structure of embreyite. In the disordered interlayer, there is one split Pb2 site and one low occupancy Cu1 position.

Heteropolyhedral layer

The Pb1 site adopts a 6-fold coordination in the first coordination sphere with six short and strong Pb1–O bonds with the average <Pb1–O_6> bond distance of 2.63 Å (Table 5). The resultant $Pb1O_6$ polyhedron can be described as a distorted octahedron (Fig. 4*a*). There are six more additional oxygen atoms located at larger distances from 3.24 to 3.29 Å thus forming distorted $Pb1O_{12}$ cuboctahedron. The average <Pb1–O_{12}> bond length of the 12-coordinated Pb1-centred polyhedron is 2.94 Å.

One symmetrically independent tetrahedral *T* site is surrounded by four O atoms (Fig. 4*b*). Calculations of the mineral formula on the basis of O = 4 apfu provided the sum of tetrahedral cations ($Cr^{6+}_{0.52}$ and $P^{5+}_{0.43}$) is < 1. The latter prompted us to consider this site as partially occupied. Unconstrained refinement of the occupancies of the *T* site led to ($Cr_{0.520}P_{0.432}\square_{0.048}$). Structural models containing partially occupied tetrahedral sites were reported previously for minerals and synthetic compounds, e.g. in byzantievite, $Ba_5(Ca,REE,Y)_{22}(Ti,Nb)_{18}(SiO_4)_4[(PO_4),(SiO_4)]_4(BO_3)_9O_{21}[(OH),F]_{43}(H_2O)_{1.5}$ (*REE* = rare-earth minerals) (Sokolova *et al.*, 2010) and synthetic $AMo_3P_{5.8}Si_2O_{25}$ (*A* = Rb or Tl^+) (Leclaire *et al.*, 1984), where a deficiency of P^{5+} is observed in PO_4 groups to make the formula electroneutral. To the best of our knowledge the crystal structure of embreyite is the first observation in minerals of a

TABLE 5. Selected interatomic distances in Å in the structure of embreyite.

Pb1–O2	2.625(13) × 2	Cu1–O1	2.234(9) × 4
Pb1–O1	2.635(9) × 4		
<Pb1–O_6>	2.632	Pb2A–Pb2B	0.998(3)
Pb1–O3	3.240(8) × 4	Pb2A–Pb2C	1.029(6)
Pb1–O3^{i}	3.286(16) × 2	Pb2A–Cu1	1.856(5)
<Pb1–O_{12}>	2.943		
		T–O3	1.576(12)
Pb2A–O3	2.399(12)	*T*–O1	1.588(9) × 2
Pb2A–O1	2.828(10) × 2	*T*–O2	1.594(14)
Pb2A–O2	2.873(5) × 2	<*T*–O_4>	1.587
Pb2A–O1^{ii}	2.948(11) × 2		
Pb2A–O1^{iii}	2.980(10) × 2		
Pb2A–O2^{iv}	3.013(15)		
<Pb2A–O_{10}>	2.867		

Symmetry codes: (i) –x+1, –y, –z + 1; (ii) x + ½, –y + ½, z; (iii) –x + 1, –y + 1, –z + 2; (iv) –x + 3/2, –y + ½, –z + 2.

https://doi.org/10.1180/minmag.2017.081.041 Published online by Cambridge University Press

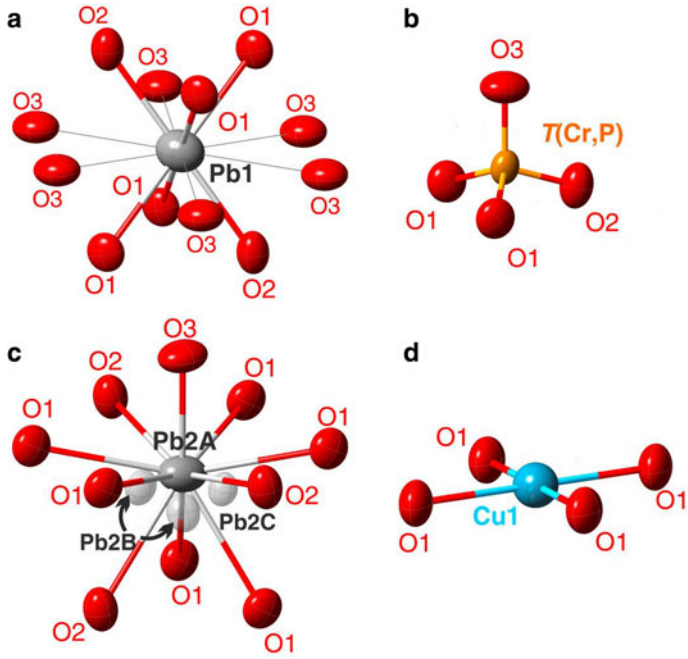

FIG. 4. Geometry of the cationic sites in the crystal structure of embreyite. Displacement ellipsoids are drawn at the 50% probability level.

mixed tetrahedral site occupied by Cr^{6+} and P^{5+}. The bond-valence sum (BVS) calculations for the *T* site confirm a mixed 5+/6+-valence occupancy providing the weighted bond-valence sum of 5.52 valence units (vu). The average <*T*–O> bond length value is 1.59 Å.

Disordered interlayer

The Pb2 site is split over Pb2A, Pb2B and Pb2C positions in the crystal structure of embreyite. Disorder of Pb atoms in the interlayer is rather typical for lead oxysalt layered structures and has been reported e.g. for hydrocerussite (Martinetto *et al*., 2002), rickturnerite (Rumsey *et al*., 2012) and $Pb_{21}[Si_7O_{22}]_2[Si_4O_{13}]$ (Siidra *et al.*, 2014*b*). Refinement of the occupancies of the three Pb2 sites with the total occupancy of 0.605 revealed the presence of a vacancy here. Most probably, it can be filled by H_2O molecules evidenced by the presence of typical absorption bands at ~3300 and ~1600 cm^{-1} in the IR spectrum (Fig. 2). We suggest that the disordered Pb2 sites are the only possible sites for H_2O in the structure of embreyite as we were unable to find other prominent peaks on difference-Fourier maps that could be interpreted as positions of water molecules. A similar example of complicated water site localization has been reported recently for gianellaite, $[(NHg_2)_2](SO_4)(H_2O)_x$ (Cooper *et al*., 2016) where H_2O could not be localized in the latter from structural data. However, the presence of water was undoubtedly indicated by absorption bands in the IR spectra.

The most electron-dense Pb2A site is symmetrically coordinated by ten O atoms located at distances varying from 2.40 to 3.01 Å with the average <$Pb2A–O_{10}$> bond distance of 2.87 Å (Fig. 4*c*).

The chemical analysis reveals $Cu^{2+}_{0.07}$ pfu. A small amount of copper was assigned to the Cu1 site, which can be also considered as one of the Pb2 split positions. Geometrical analysis demonstrates square coordination environments for the Cu1 site (Fig. 4*d*) with oxygen atoms located at a distance of 2.23 Å. However, these long bond-distance values should not be considered literally due to the strong disorder. We suggest that the Cu1 site is the most favoured position for a small amount of Cu in the crystal structure of embreyite because of its typical square coordination environment and structural relation with vauquelinite, discussed below.

The final refinement of the structure of embreyite led to the structural formula of $[Pb_{0.794}Cu_{0.066}$

https://doi.org/10.1180/minmag.2017.081.041 Published online by Cambridge University Press

$\square_{0.140-x}$]{[$Pb_{0.500}$][($Cr_{0.520}P_{0.432}\square_{0.048}$)$O_4$)]}$(H_2O)_n$ (the presence of H_2O is assumed by IR data), which is in a good agreement with the electron microprobe data on the basis of 4 O atoms per formula unit, i.e. $(Pb_{0.79(1)}Cu_{0.07(2)})_{\Sigma 0.86}(Pb_{0.50(2)})_{\Sigma 0.5}(Cr_{0.52(2)}P_{0.43(2)})_{\Sigma 0.95}O_4$.

Crystal structure: description and comparison with palmierite-type compounds

The crystal structure of embreyite is based on {Pb[(Cr,P)O_4]$_2$]} layers formed by corner-sharing mixed chromate–phosphate tetrahedra and Pb-centred polyhedra (Fig. 5*a*). The interlayer space is filled by disordered Pb^{2+} and Cu^{2+} cations. Generally, the crystal structure of embreyite can be referred to the structural type of palmierite, $K_2Pb(SO_4)_2$ (Moore, 1973; Tissot *et al*., 2001) built up from stacking of layers parallel to (001) and formed by corner-sharing distorted Pb^{2+} polyhedra and SO_4 tetrahedra with K^+ cations in the interlayer. A variety of cations in different oxidation states are involved in homovalent or heterovalent substitutions observed in the large number of palmierite-type structures with different structural distortions (Lazoryak, 1996).

It is worth considering the low-temperature rhombohedral modification of $Pb_4(PO_4)_2(CrO_4)$ chemically close to embreyite that has been studied by neutron powder diffraction (Barbier and Maxin, 1995). The rhombohedral structure of $Pb_4(PO_4)_2(CrO_4)$ ($R\bar{3}m$, $a = 5.5403(1)$, $c = 20.4999(4)$ Å and $V = 544.94(1)$ Å^3) is based upon stacking along the c axis of layers composed of (P,Cr)O_4 and PbO_{12} polyhedra with partially occupied Pb^{2+} sites in the interlayer space, similar to the palmierite-type monoclinic structure of embreyite (Fig. 5*b*). The structural formula of the rhombohedral modification of $Pb_4(PO_4)_2(CrO_4)$ according to the published data can be written as $2 \times [Pb_{0.83}\square_{0.17}][Pb_{0.5}(PO_4)_{0.67}(CrO_4)_{0.33}]$, similar to the one determined for embreyite, $[Pb_{0.794}Cu_{0.066}\square_{0.140-x}]$ {$[Pb_{0.500}][(Cr_{0.520}P_{0.432}\square_{0.048})O_4)]$}$(H_2O)_n$. Another palmierite-type compound with disordered cation sites is $Sr_{2.67}\square_{0.33}(PO_4)_{1.33}(CrO_4)_{0.67}$ (Hartl and Braungart, 1978*a*,*b*). It has a large supercell with a doubling of both the a and c edges ($R\bar{3}m$, $a = 10.91$ and $c = 39.78$ Å) which most probably results from ordering of vacancies in the crystal structure. Note that, palmierite-type $(Pb,Ba)_3(PO_4)_2$ phases structurally related to embreyite were studied previously as ferroelastic materials exhibiting the $R\bar{3}m$ to $C2/c$ ferroelastic transition around $T = 180$°C, and were considered as model compounds for ferroelastic distortions (Bismayer and Salje, 1981; Aktas *et al*., 2013; Salje, 2015).

Discussion

Lead chromate minerals

There are 13 lead chromate minerals approved by the International Mineralogical Association to date (Table 1). The crystal structures of cassedanneite $Pb_5(VO_4)_2(CrO_4)_2{\cdot}H_2O$ (Cesbron *et al*., 1988) (see below) and santanaite $Pb_9^{2+}Pb_2^{4+}O_{12}(CrO_4)$ (Mücke, 1972) remain unknown to date. Some of those studied by single-crystal XRD gave poor quality structure refinements for various different reasons: fornacite had $R_1 = 0.10$ (Cocco *et al*., 1967); reynoldsite, $R_1 = 0.10$ (Kampf *et al*., 2012*b*); and vauquelinite, $R_1 = 0.09$ (Fanfani and Zanazzi, 1968). Macquartite, $Pb_7Cu_2(CrO_4)_4(SiO_4)_2(OH)_2$ (Williams and Duggan, 1980) was not studied by single-crystal XRD but assumed to be isostructural with wherryite, $Pb_7Cu_2(SO_4)_4(SiO_4)_2(OH)_2$ (Cooper and Hawthorne, 1994). Lead-containing minerals or synthetic compounds with bichromate $(Cr_2O_7)^{2-}$ groups are unknown. The CrO_4 tetrahedra are isolated in all Pb chromate mineral crystal structures. Most of these minerals (except crocoite, georgerobinsonite and phoenicochroite) contain AO_6 polyhedra with different types of connectivity modes with CrO_4 tetrahedra *via* common oxygen atoms. CrO_4 groups are monodentate with CuO_6 octahedra in the structure of fornacite and vauquelinite. The structures of hemihedrite and iranite contain CrO_4 groups shared with ZnO_6 (hemihedrite) or CuO_6 (iranite) octahedra also in monodentate mode. However, chromate groups are only shared with Pb-centred polyhedra and do not have common oxygen vertices with TeO_6 and MnO_6 octahedra in the structures of chromschieffelinite and reynoldsite, respectively.

Formula of embreyite

The structural formula obtained for the embreyite sample studied, $[Pb_{0.794}Cu_{0.066}\square_{0.140-x}]$ {$[Pb_{0.500}][(Cr_{0.520}P_{0.432}\square_{0.048})O_4)]$}$(H_2O)_n$, is in general agreement with that assumed earlier for this mineral on the basis of different data, $Pb_2[Pb_xM_y^{2+}\square_{1-x-y}]_1(CrO_4)(PO_4)(OH_{2(x+y)-1},H_2O,\square)_{\Sigma 1}$, where $M^{2+} = Cu$, Zn and $0.5 \le x + y \le 1$, or $Pb_2(M,\square)(CrO_4)(PO_4)X$, where $M = Pb$, Cu and Zn and $X = OH$, H_2O and $\square$ (Khanin *et al*., 2015). The

https://doi.org/10.1180/minmag.2017.081.041 Published online by Cambridge University Press

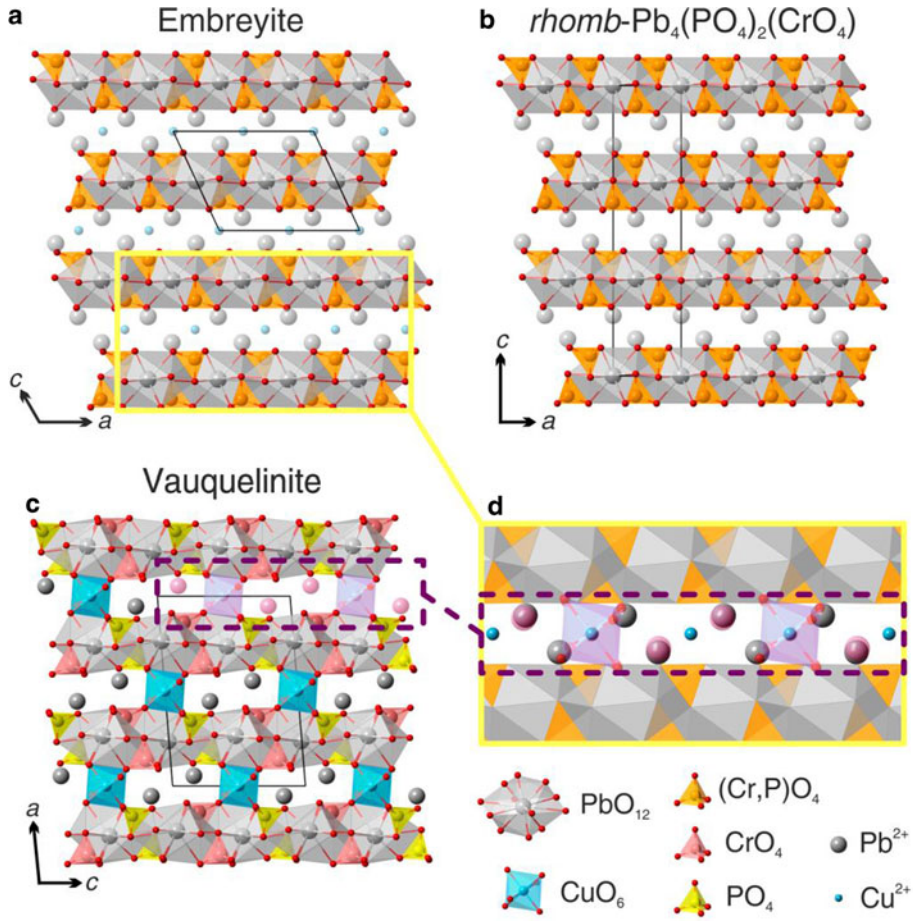

FIG. 5. General views of the crystal structures of (*a*) embreyite, (*b*) synthetic *rhomb*-$Pb_4(PO_4)_2CrO_4$ and (*c*) vauquelinite. Projection of the interlayer block of the structure of vauquelinite on the structure of embreyite is shown in (*d*).

major discrepancy between them is in the presentation of the tetrahedrally coordinated constituents: the structure determination revealed Cr–P disorder. The results of the structure determination suggest attributing the M^{2+} cations to the second disordered Pb position. Thus, the generalized formula of embreyite can be represented as $(Pb_xM_y^{2+}\square_{1-x-y})_2\{Pb[(Cr,P)O_4]_2\}(H_2O)_n$, where M^{2+} = Cu, Zn and $0.5 \leq x+y \leq 1$, or, in simplified form: $(Pb,Cu,\square)_2\{Pb[(Cr,P)O_4]_2\}(H_2O)_n$. Minor amounts of vacancies in the tetrahedral site are ignored in the formula for simplification. The powder XRD patterns of the holotype embreyite (Williams, 1972) and our material are close in both *d* values and intensities of reflections. This observation became a reason to re-calculate unit-cell parameters for the holotype sample (due to minor differences in the unit-cell of our sample in the *c* dimension and β angle values) using our cell setting and corresponding *hkl* indices. Unit-cell parameters and volume obtained for the holotype are very close to those of the embreyite sample described in this present investigation. We recommend this unit-cell setting (with β ≈ 114–115° instead of the original β ≈ 104°) and *hkl* indices for the reflections from powder XRD as given in Table 2 for embreyite in general.

Comparison with yavapaiite-type minerals and synthetic compounds

The layers of $\{Pb[(Cr,P)O_4]_2]\}$ in embreyite are similar in topology to those in yavapaiite-type

https://doi.org/10.1180/minmag.2017.081.041 Published online by Cambridge University Press

compounds, e.g. brianite $Na_2Ca[Mg(PO_4)_2]$ (Alkemper and Fuess, 1998) and steklite $KAl(SO_4)_2$ (Murashko *et al.*, 2013). The tetrahedron acts as a tridentate-bridging ligand thus leaving its fourth vertex (O_t) as terminal or non-shared and in orientation towards the interlayer space in yavapaiite (Fig. 6*a*). O_t are directed into the layer (Fig. 6*b*) in embreyite. O_t atoms provide the linkage of heteropolyhedral layers with interlayer cations in yavapaiite. However all three O atoms of basal triangular planes of tetrahedra are involved in strong bonding with interlayer cations in embreyite. In this sense the structural architecture of heteropolyhedral layers in embreyite is similar to those of bütschliite-type compounds (Fig. 6*c*), e.g. $K_2Mg(CO_3)_2$ (Hesse and Simons, 1982) and $KBaY(BO_3)_2$ (Gao *et al.*, 2011), where the tetrahedra are replaced by triangles of carbonate or borate groups with a similar method of bonding with interlayer species. Another type of layer related to heteropolyhedral blocks in embreyite was described previously in the structures of markhininite, $TlBi(SO_4)_2$ (Siidra *et al.*, 2014*a*) and synthetic, $RbEu(SO_4)_2$ (Sarukhanyan *et al.*, 1983). A^{3+}-centred (A = Bi or REE^{3+}) polyhedra share edges with adjacent SO_4 tetrahedra in contrast to the other yavapaiite-type compounds with corner-sharing octahedra and tetrahedra in heteropolyhedral blocks. Such coordination of sulfate groups leads to more densely packed layered units and, consequently, orientation of the fourth oxygen vertex towards the layer (Fig. 6*d*). Note, there is also a group of Se-

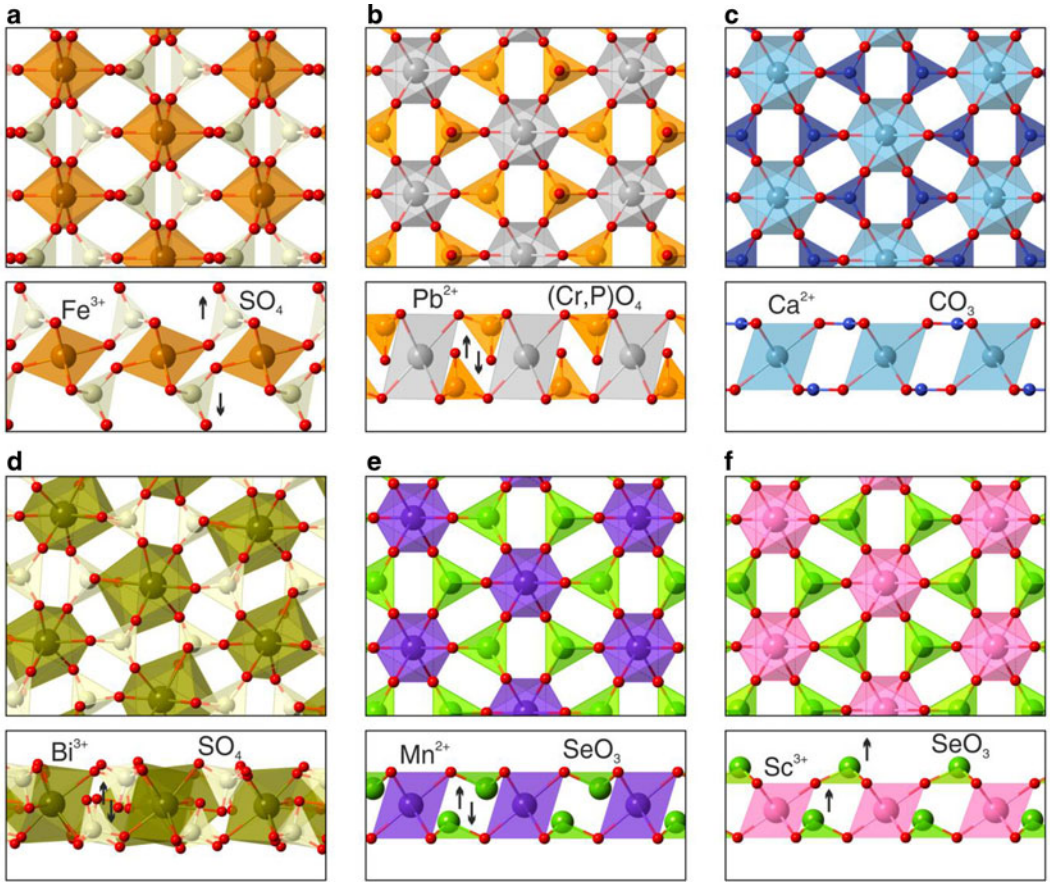

FIG. 6. Heteropolyhedral yavapaiite-related layers in minerals and synthetic compounds: (*a*) yavapaiite $KFe(SO_4)_2$, (*b*) embreyite, (*c*) bütschliite $K_2Ca(CO_3)_2$, (*d*) markhininite $TlBi(SO_4)_2$, (*e*) $K_2Mn(SeO_3)_2$ and (f) $RbSc(SeO_3)_2$. Black arrows designate the orientation of TO_4 tetrahedra or SeO_3 groups in a direction towards or outwards from the layer. See the text for details.

https://doi.org/10.1180/minmag.2017.081.041 Published online by Cambridge University Press

containing phases related to both yavapaiite- and bütschliite-type compounds. Apical vertices of triangular selenite $Se^{4+}O_3$ pyramids are oriented into the centre of the layers identically to $(Cr,P)O_4$ groups in embreyite (Fig. 6*e*) in the crystal structures of $K_2M(SeO_3)_2$ compounds [M^{2+} = Mg (Hesse and Simons, 1982), Co (Wildner, 1992*a*) and Mn (Wildner, 1992*b*)], whereas the apices of the pyramids are aligned one by one in the same direction emphasizing a non-centrosymmetric character in β-$PbNi(SeO_3)_2$ (Kovrugin *et al*., 2015) and $RbSc(SeO_3)_2$ (Song and Ok, 2015) (Fig. 6*f*).

Comparison with vauquelinite

It is of interest to examine and compare the chemical features and structural architectures of embreyite with vauquelinite, ideally $Pb_2Cu(CrO_4)(PO_4)(OH)$ (Fanfani and Zanazzi, 1968; Cesbron and Williams, 1980), as they form a continuous solid-solution series with the Pb:Cu ratio as the main varying value (Khanin *et al*., 2015) regardless of significant structural differences. The data from EMPA and powder XRD demonstrate the existence of the margin between these phases as approximately between 0.5 and 0.6 apfu of Cu in the idealized formula of vauquelinite. The recommended simplified formula of embreyite, $(Pb,Cu,\square)_2\{Pb[(Cr,P)O_4]_2\}(H_2O)_n$, demonstrates definite similarity in stoichiometry with the vauquelinite formula and explains the existence of the solid-solution series. The Pb:Cu ratio in the point of nucleation of a crystal in a phosphate–chromate mineral-forming system may determine a mineral form (embreyite/vauquelinite) to be crystallized. This may explain the cause and mechanism of the formation of botryoidal aggregates and encrustations up to several mm thick composed by alternating layers of vaquelinite and embreyite (Fig. 7). Such interstratified bi-mineral aggregates are very typical for the chromate assemblages at the Berezovskoe deposit (Williams, 1972; Kleymenov *et al*., 2003; Khanin *et al*., 2015). We believe that they may form as a result of oscillatory crystallization processes in the systems chemically close to the margin between the stability fields of embreyite and vauquelinite defined by the Pb:Cu ratio.

Vauquelinite and embreyite demonstrate different, but related, structure types. The former is very close structurally to brackebuschite-group minerals with a crystal structure (Cesbron and Williams, 1980) based on columns of edge-sharing $CuO_4(OH)_2$ octahedra oriented along the *b* axis. CrO_4 and PO_4 tetrahedra are shared with octahedra *via* monodentate bridging of one of four oxygen vertices. Pb^{2+} cations are located in between the columns and provide three-dimensional integrity of the structure. A closer look at the coordination environments of one of two Pb sites in vauquelinite reveals similarity with the Pb1-centred coordination polyhedron in embreyite. It can be described as a distorted cuboctahedron with six short Pb–O distances (2.40–2.94 Å) and six longer ones (3.01–3.63 Å). PbO_{12}, PO_4 and CrO_4 polyhedra form heteropolyhedral layers in vauquelinite similar to those in embreyite. Additional Cu^{2+} and Pb^{2+} cations provide the linkage of these blocks (Fig. 5*c*) in vauquelinite. The common structural motif of vauquelinite and embreyite suggests the possible location of a small amount of Cu in the structure of the latter in the interlayer space. Embreyite can be considered as an intermediate phase between the structures of vauquelinite and rhombohedral modification of $Pb_4(PO_4)_2(CrO_4)$ (unknown as a mineral), where the disordered interlayer species are represented by a superposition of ordered cations in two different structures related to each other by translation (Fig. 5*d*).

There is also a link between the lattice dimensions of these minerals (Table 6). The unit-cell parameters of embreyite are close to those of the brackebuschite-related minerals, e.g. tsumebite $Pb_2Cu(PO_4)(SO_4)(OH)$ and arsentsumebite $Pb_2Cu(AsO_4)(SO_4)(OH)$ (Fanfani and Zanazzi, 1968; Zubkova *et al*., 2002). Remarkably, vauquelinite

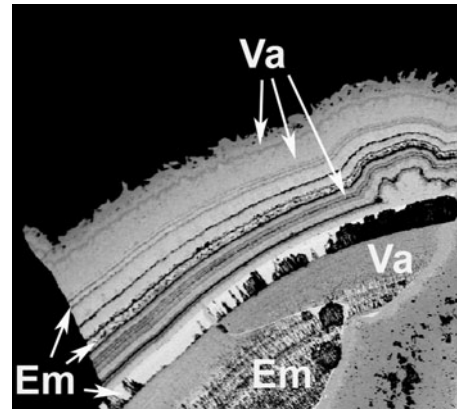

FIG. 7. Back-scattered electron image showing rhythmically zoned crust consisting of embreyite (Em) and vauquelinite (Va) layers. Berezovskoe deposit, Urals, Russia. Sample #10393 in the systematic collection of Fersman Mineralogical Museum of the Russian Academy of Sciences, Moscow. Field of view: width = 1.9 mm.

https://doi.org/10.1180/minmag.2017.081.041 Published online by Cambridge University Press

TABLE 6. Crystallographic parameters of vauquelinite, fornacite, tsumebite and embreyite.

Mineral	Formula	Sp. gr.	Z	a (Å)	b (Å)	β (°)	c (Å)	V (Å^3)	Ref.
Vauquelinite*	$Pb_2Cu(CrO_4)(PO_4)(OH)$	$P2_1/n$	4	16.110	5.806	110.47	17.366	1521.7	[1]
Fornacite	$Pb_2Cu(CrO_4)(AsO_4)(OH)$	$P2_1/c$	4	8.090	5.909	110.0	17.484	785.5	[2]
Tsumebite	$Pb_2Cu(PO_4)(SO_4)(OH)$	$P2_1/m$	2	7.850	5.800	111.0	8.700	369.8	[3]
Embreyite	$(Pb,Cu,\square)_2\{Pb[(Cr,P)O_4]_2\}(H_2O)_n$	$C2/m$	1	9.802	5.603	114.9	7.649	381.2	[4]

References: [1] – Fanfani and Zanazzi (1968); [2] – Ksenofontov *et al.* (2014); [3] – Nichols (1966); [4] – this work.
*Unit cell was transformed with a and c axes chosen as the [101] and [10$\bar{1}$] directions, respectively, in the original unit-cell reported by Fanfani and Zanazzi (1968) [a = 13.754(5), b = 5.806(6), c = 9.563(3) Å, β = 94.57(17)° and V = 761.2 Å^3].
Sp. gr. – space group.

and fornacite also belong to the brackebuschite structural family and exhibit doubling of both a and c unit-cell parameters in the former, and the c parameter in the latter. Structural relationships are confirmed by the above-discussed genetic linkage between vauquelinite and embreyite.

Final remarks

The determination of the embreyite structure may help to suggest the crystal chemical nature of cassedanneite. This mineral has also been discovered in an old museum specimen from Berezovskoe. However, to date, no crystals suitable for a structural study are known. Cassedanneite is similar in stoichiometry and powder XRD pattern to embreyite and was considered previously to be an analogue with the VO_4^{3-} anion instead of PO_4^{3-}. The idealized formula of cassedanneite was suggested as $Pb_5(CrO_4)_2(VO_4)_2{\cdot}H_2O$; the holotype of this mineral contains 0.61 wt.% CuO and 0.65 wt.% ZnO (Cesbron *et al.*, 1988) not included in the simplified formula. Our recent data for another specimen of cassedanneite from the same locality show up to 3.8 wt.% CuO, concentrations that are similar to those in embreyite. We propose that the structural similarity of cassedanneite and embreyite is related to the disordered distribution of Cr and V. This character of disorder seems to be very likely taking into account the following observations: (1) the existence of the continuous solid-solution series of the brackebuschite-type minerals between vauquelinite $Pb_2Cu(CrO_4)(PO_4)(OH)$, bushmakinite $Pb_2Al(VO_4)(PO_4)(OH)$, ferribushmakinite $Pb_2Fe^{3+}(VO_4)(PO_4)(OH)$ and a phase with the hypothetical end-member composition of $Pb_2Cu(VO_4)(PO_4)(H_2O)$. The major substitution scheme is $Cr^{6+} + Cu^{2+} \leftrightarrow V^{5+} + (Al,Fe)^{3+}$ (Khanin and Pekov, 2016*a*,*b*). (2) The crystal chemical similarity between Cr^{6+} and V^{5+} metals is closer than between Cr^{6+} and P^{5+}.

Our recently obtained data demonstrate that the powder XRD pattern of cassedanneite contains a distinct reflection with d = 13.9 Å, forbidden for the embreyite unit cell (see Table 2). This feature may indicate the doubling of the c unit-cell parameter of cassedanneite in comparison with embreyite, which may explain the structural differences between these two minerals.

Hexagonal relationships observed for embreyite and rhombohedral $Pb_4(PO_4)_2(CrO_4)$ indicates the possibility of phase transitions. The behaviour of embreyite at higher temperatures may be somewhat similar to the reported leadhillite → susannite

https://doi.org/10.1180/minmag.2017.081.041 Published online by Cambridge University Press

($P2_1/a \rightarrow P3$) transition at 85°C (Bindi and Menchetti, 2005; Steele *et al*., 1998) explained by the changes in orientation of sulfate tetrahedra and PbO_n coordination polyhedra. However, the absence to date of pure embreyite material in sufficient quantities prevents additional studies.

Acknowledgements

The authors thank Joël Brugger and one anonymous reviewer for valuable comments and very helpful remarks that improved the manuscript. This study was supported by the Russian Science Foundation, grants nos. 16-17-10085 (XRD and structural studies) and 14-17-00048 (mineralogical investigations). The technical support by the SPbSU X-Ray Diffraction Resource Center is acknowledged.

References

Adib, D. and Ottemann, J. (1970) Some new lead oxide minerals and murdochite from T. Khuni Mine, Anarak, Iran. *Mineralium Deposita*, **5**, 86–93.

Aktas, O., Salje, E.K.H. and Carpenter, M.A. (2013) Resonant ultrasonic spectroscopy and resonant piezoelectric spectroscopy in ferroelastic lead phosphate, $Pb_3(PO_4)_2$. *Journal of Physics: Condensed Matter*, **25**, 465401.

Alkemper, J. and Fuess, H. (1998) The crystal structures of $NaMgPO_4$, $Na_2CaMg(PO_4)_2$ and $Na_{18}Ca_{13}Mg_5(PO_4)_{18}$: new examples for glaserite related structures. *Zeitschrift für Kristallographie – Crystalline Materials*, **213**, 282–287.

Barbier, J. and Maxin, D. (1995) Phase transformation in $Pb_4(PO_4)_2CrO_4$. *Journal of Solid State Chemistry*, **116**, 179–184.

Bariand, P. and Herpin, P. (1963) Une nouvelle espèce minérale: l'iranite, chromate hydraté de plomb. *Bulletin de la Societe Francaise Mineralogie et de Cristallographie*, **86**, 113–135.

Bindi, L. and Menchetti, S. (2005) Structural changes accompanying the phase transformation between leadhillite and susannite: A structural study by means of *in situ* high-temperature single-crystal X-ray diffraction. *American Mineralogist*, **90**, 1641–1647.

Bismayer, U. and Salje, E. (1981) Ferroelastic phases in $Pb_3(PO_4)_2$–$Pb_3(AsO_4)_2$; X-ray and optical experiments. *Acta Crystallographica*, **A37**, 145–153.

Cesbron, F. and Williams, S.A. (1980) Iranite-hémihédrite, bellite, phoenicochroite, vauquelinite et fornacite: synthèse et nouvelles données. *Bulletin de Minéralogie*, **103**, 469–477.

Cesbron, F., Giraud, R., Pillard, F. and Poullen, J.-F. (1988) La cassedannéite, nouveau chromo-vanadate de plomb de Beresovsk (Oural). *Comptes Rendus de l'Académie des Sciences – Series II*, **306**, 125–127.

Christy, A. (2015) Causes of anomalous mineralogical diversity in the Periodic Table. *Mineralogical Magazine*, **79**, 33–49.

Chukanov, N.V. and Chervonnyi, A.D. (2016) *Infrared Spectroscopy of Minerals and Related Compounds*. Springer Verlag, Cham, Switzerland.

Cocco, G., Fanfani, L. and Zanazzi, P.F. (1967) The crystal structure of fornacite. *Zeitschrift für Kristallographie*, **124**, 385–397.

Cooper, M.A. and Hawthorne, F.C. (1994) The crystal structure of wherryite, $Pb_7Cu_2(SO_4)_4(SiO_4)_2(OH)_2$, a mixed sulfate-silicate with $[^{[6]}M(TO_4)_2\phi]$ chains. *The Canadian Mineralogist*, **32**, 373–380.

Cooper, M.A., Ball, N.A., Hawthorne, F.C., Paar, W.H., Roberts, A.C. and Moffatt, E. (2011) Georgerobinsonite, $Pb_4(CrO_4)_2(OH)_2FCl$, a new chromate mineral from the Mammoth – St. Anthony mine, Tiger, Pinal County, Arizona: description and crystal structure. *The Canadian Mineralogist*, **49**, 865–876.

Cooper, M.A., Abdu, Y.A., Hawthorne, F.C. and Kampf, A.R. (2016) The crystal structure of gianellaite, $[(NHg_2)_2](SO_4)(H_2O)_x$, a framework of (NHg_4) tetrahedra with ordered (SO_4) groups in the interstices. *Mineralogical Magazine*, **80**, 869–875.

Effenberger, H. and Pertlik, F. (1986) Four monazite type structures: comparison of $SrCrO_4$, $SrSeO_4$, $PbCrO_4$ (crocoite), and $PbSeO_4$. *Zeitschrift für Kristallographie*, **176**, 75–83.

Fanfani, L. and Zanazzi, P.F. (1968) The crystal structure of vauquelinite and the relationships to fornacite. *Zeitschrift für Kristallographie – Crystalline Materials*, **126**, 433–443.

Fettes, D. and Desmons, J. (2007) *Metamorphic rocks – A Classification and Glossary of Terms*. Cambridge University Press, UK.

Gao, J., Song, L., Hu, X. and Zhang, D. (2011) A buetschliite-type rare-earth borate, $KBaY(BO_3)_2$. *Solid State Sciences*, **13**, 115–119.

Hartl, K. and Braungart, R. (1978*a*) Strontiumchromat(V, VI), $Sr_{2.67}\square_{0.33}(CrO_4)_{1.33}(CrO_4)_{0.67}$, eine Hochtemperaturphase mit Defekt-Bariumphosphat-Struktur. *Zeitschrift für Naturforschung*, **B33**, 952–953 [in German].

Hartl, K. and Braungart, R. (1978*b*) Strontiumphosphat-chromat(VI), $Sr_3(PO_4)_2{\cdot}SrCrO_4$, eine dimorphe Hochtemperaturverbindung. *Zeitschrift für Naturforschung*, **B33**, 954–955 [in German].

Hesse, K.-F. and Simons, B. (1982) Crystal structure of synthetic $K_2Mg(CO_3)_2$. *Zeitschrift für Kristallographie*, **161**, 289–292.

Kampf, A.R., Mills, S.J., Housley, R.M., Rumsey, M.S. and Spratt, J. (2012*a*) Lead-tellurium oxysalts from Otto Mountain near Baker, California: VII. Chromschieffelinite, $Pb_{10}Te_6O_{20}(OH)_{14}(CrO_4)$

https://doi.org/10.1180/minmag.2017.081.041 Published online by Cambridge University Press

$(H_2O)_5$, the chromate analog of schieffelinite. *American Mineralogist*, **97**, 212–219.

Kampf, A.R., Mills, S.J., Housley, R.M., Bottrill, R.S. and Kolitsch, U. (2012*b*) Reynoldsite, $Pb_2Mn_2^{4+}O_5(CrO_4)$, a new phyllomanganate-chromate from the Blue Bell claims, California and the Red Lead mine, Tasmania. *American Mineralogist*, **97**, 1187–1192.

Khanin, D.A. and Pekov, I.V. (2016*a*) Minerals with brackebuschite-like structures: a novel solid-solution system involving Cr^{6+} and V^{5+}. *Zapiski Rossiiskogo Mineralogicheskogo Obshchestva*, **145**, 96–112 [in Russian].

Khanin, D.A. and Pekov, I.V. (2016*b*) New data on cassedanneite. *International Conference Dedicated to 300-year Anniversary of the Fersman Mineralogical Museum*. Moscow, pp. 188–189 [in Russian].

Khanin, D.A., Pekov, I.V., Pakunova, A.V., Ekimenkova, I.A. and Yapaskurt, V.O. (2015) Natural system of fornacite–vauquelinite–embreyite solid solutions and variations in the chemical composition of these minerals from occurrences of the Urals. *Zapiski Rossiiskogo Mineralogicheskogo Obshchestva*, **144**, 36–60 [in Russian].

Kleymenov, D.A., Pekov, I.V., Erokhin, Y.V. and Chukanov, N.V. (2003) New data on embreyite from the oxidation zone of the Berezovskoye gold deposit. Pp. 171–177 in: *Mineralogiya Urala-2003*. Miass, Russia [in Russian].

Kovrugin, V.M., Colmont, M., Terryn, C., Colis, S., Siidra, O.I., Krivovichev, S.V. and Mentré, O. (2015) pH-Controlled pathway and systematic hydrothermal phase diagram for elaboration of synthetic lead nickel selenites. *Inorganic Chemistry*, **54**, 2425–2434.

Ksenofontov, D.A., Kabalov, Y.K., Pekov, I.V., Zubkova, N.V., Ekimenkova, I.A. and Pushcharovskii, D.Y. (2014) Refinement of the crystal structure of fornacite using the Rietveld method. *Doklady Earth Sciences*, **456**, 520–523.

Lazoryak, B.I. (1996) Design of inorganic compounds with tetrahedral anions. *Russian Chemical Reviews*, **65**, 287–305.

Leclaire, A., Monier, J.C. and Raveau, B. (1984) A molybdosilicophosphate with an intersecting-tunnel structure which exhibits ion-exchange properties, $AMo_3P_{5.8}Si_2O_{25}$ (A = Rb, Tl). *Acta Crystallographica*, **B40**, 180–185.

Martinetto, P., Anne, M., Dooryhée, E., Walter, P. and Tsoucaris, G. (2002) Synthetic hydrocerussite, $2PbCO_3 \cdot Pb(OH)_2$, by X-ray powder diffraction, *Acta Crystallographica*, **C58**, i82–i84.

McLean, W.J. and Anthony, J.W. (1970) The crystal structure of hemihedrite. *American Mineralogist*, **55**, 1103–1114.

Moore, P.B. (1973) Bracelets and pinwheels: A topological-geometrical approach to the calcium orthosilicate and alkali sulfate structures. *American Mineralogist*, **58**, 32–42.

Mücke, A. (1972) Santanait, ein neues Bleichromat-Mineral. *Neues Jahrbuch für Mineralogie, Monatshefte*, **10**, 455–458.

Murashko, M.N., Pekov, I.V., Krivovichev, S.V., Chernyatyeva, A.P., Yapaskurt, V.O., Zadov, A.E. and Zelensky, M.E. (2013) Steklite, $KAl(SO_4)_2$: A finding at the Tolbachik Volcano, Kamchatka, Russia, validating its status as a mineral species and crystal structure. *Geology of Ore Deposits*, **55** [Special Issue: *Rossiiskogo Mineralogicheskogo Obshchestva*], 594–600.

Nakamoto, K. (2009) *Infrared and Raman Spectra of Inorganic and Coordination Compounds, Part B, Applications in Coordination, Organometallic, and Bioinorganic Chemistry.* John Wiley & Sons, Hoboken, USA.

Nichols, M.C. (1966) The structure of tsumebite. *American Mineralogist*, **51**, 267–267.

Pekov, I.V. (1998) *Minerals First Discovered on the Territory of the Former Soviet Union*. OP, Moscow.

Quareni, S. and de Pieri, R. (1965) A three-dimensional refinement of the structure of crocoite, $PbCrO_4$. *Acta Crystallographica*, **19**, 287–289.

Rumsey, M.S., Krivovichev, S.V., Siidra, O.I., Kirk, C.A., Stanley, C.J. and Spratt, J. (2012) Rickturnerite, $Pb_7O_4[Mg(OH)_4](OH)Cl_3$, a complex new lead oxychloride mineral. *Mineralogical Magazine*, **76**, 59–73.

Salje, E.K.H. (2015) Modulated minerals as potential ferroic materials. *Journal of Physics: Condensed Matter*, **27**, 305901.

Sarukhanyan, N.L., Iskhakova, L.D. and Trunov, V.K. (1983) Crystal structure of $RbEu(SO_4)_2$. *Kristallografiya*, **28**, 452–456 [in Russian].

Sheldrick, G.M. (2015) Crystal structure refinement with SHELXL. *Acta Crystallographica*, **C71**, 3–8.

Siidra, O.I., Vergasova, L.P., Krivovichev, S.V., Kretser, Y. L., Zaitsev, A.N. and Filatov, S.K. (2014*a*) Unique thallium mineralization in the fumaroles of Tolbachik volcano, Kamchatka Peninsula, Russia. I. Markhininite, $TlBi(SO_4)_2$. *Mineralogical Magazine*, **78**, 1687–1698.

Siidra, O.I., Zenko, D.S., Krivovichev, S.V. (2014*b*) Structural complexity of lead silicates: Crystal structure of $Pb_{21}[Si_7O_{22}]_2[Si_4O_{13}]$ and its comparison to hyttsjoite. *American Mineralogist*, **99**, 817–823.

Sokolova, E., Hawthorne, F.C., Pautov, L.A. and Agakhanov, A.A. (2010) Byzantievite, $Ba_5(Ca,REE,Y)_{22}(Ti,Nb)_{18}(SiO_4)_4[(PO_4),(SiO_4)]_4(BO_3)_9O_{21}[(OH),F]_{43}(H_2O)_{1.5}$: the crystal chemistry of the only known mineral with the oxyanions (BO_3), (SiO_4) and (PO_4). *Mineralogical Magazine*, **74**, 285–308.

Song, S.Y. and Ok, K.M. (2015) Modulation of framework and centricity: cation size effect in new quaternary selenites, $ASc(SeO_3)_2$ (A = Na, K, Rb, and Cs). *Inorganic Chemistry*, **54**, 5032–5038.

https://doi.org/10.1180/minmag.2017.081.041 Published online by Cambridge University Press

Steele, A.M., Pluth, J.J. and Livingstone, A. (1998) Crystal structure of macphersonite $Pb_4SO_4(CO_3)_2(OH)_2$: comparison with leadhillite. *Mineralogical Magazine*, **62**, 451–459.

Tissot, R.G., Rodriguez, M.A., Sipola, D.L. and Voigt, J. A. (2001) X-ray powder diffraction study of synthetic palmierite, $K_2Pb(SO_4)_2$. *Powder Diffraction*, **16**, 92–97.

Wildner, M. (1992*a*) Isotypism of a selenite with a carbonate: structure of the buetschliite-type compound $K_2Co(SeO_3)_2$. *Acta Crystallographica*, **C48**, 410–412.

Wildner, M. (1992*b*) Structure of $K_2Mn(SeO_3)_2$, a further buetschliite-type selenite. *Acta Crystallographica*, **C48**, 595.

Williams, S.A. (1972) Embreyite, a New Mineral from Berezov, Siberia. *Mineralogical Magazine*, **38**, 790–793.

Williams, S.A. and Anthony, J.W. (1970) Hemihedrite, a new mineral from Arizona. *American Mineralogist*, **55**, 1088–1102.

Williams, S.A. and Duggan, M. (1980) La macquartite: un nouveau silico-chromate de Tiger, Arizona. *Bulletin de Minéralogie*, **103**, 530–532.

Williams, S.A., McLean, W.J. and Anthony, J.W. (1970) A study of phoenicochroite – its structure and properties. *American Mineralogist*, **55**, 784–792.

Yang, H., Sano, J.L., Eichler, C., Downs, R.T. and Costin, G. (2007) Iranite, $CuPb_{10}(CrO_4)_6(SiO_4)_2(OH)_2$, isomorphous with hemihedrite. *Acta Crystallographica*, **C63**, i122–i124.

Zubkova, N.V., Pushcharovsky, D.Y., Giester, G., Tillmanns, E., Pekov, I.V. and Kleimenov, D.A. (2002) The crystal structure of arsentsumebite, $Pb_2Cu[(As,S)O_4]_2(OH)$. *Mineralogy and Petrology*, **75**, 79–88.

https://doi.org/10.1180/minmag.2017.081.041 Published online by Cambridge University Press